Electrochemical and Resonance Raman Spectroscopic Studies of Water-Oxidizing Ruthenium-Terpyridyl-Bipyridyl Complexes

Anke Keidel,[a]§ Isidoro López,[b]§ Jana Staffa,[a] Uwe Kuhlmann,[a] Fernando Bozoglian,[b] Carolina Gimbert-Suriñach,[b] Jordi Benet-Bucholz,[b] Peter Hildebrandt,*[a] and Antoni Llobet*[b][c]

§Equal contribution to the work

Abstract: The irreversible conversion of single-site water oxidation catalysts (WOC) into the more rugged catalysts structurally related to $[(trpy)(5,5'\text{-}X_2\text{-}bpy)Ru^{IV}(\mu\text{-}O)Ru^{IV}(trpy)(O)(H_2O)]^{4+}$ (X = H, **1-dn^{4+}**; X = F, **2-dn^{4+}**) represents a critical issue in developing active and durable WOC. In this work, the electrochemical and acid-base properties of **1-dn^{4+}** and **2-dn^{4+}** were evaluated. *In-situ* resonance Raman spectroscopy was employed to characterize species formed upon stoichiometric oxidation of single-site catalysts demonstrating the formation of high oxidation states mononuclear Ru=O and RuO-O complexes. Under turnover conditions, the dinuclear intermediates, **1-dn^{4+}** and **2-dn^{4+}**, as well as the previously proposed $[Ru^{VI}(trpy)(O)_2(H_2O)]^{2+}$ complex (**3^{2+}**) are formed. **3^{2+}** is a pivotal intermediate that provides access to the formation of dinuclear species. Single crystal X-ray diffraction analysis of the isolated complex $[Ru^{IV}(O)(trpy)(5,5'\text{-}F_2\text{-}bpy)]^{2+}$ reveals a clear elongation of the Ru-N bond located in the *trans* position to the oxo group, documenting the weakness of this bond which promotes the release of the bpy ligand and the subsequent formation of **3^{2+}**.

Introduction

The generation of molecular oxygen from water is one of the key challenges in contemporary chemistry and it has been in the focus of researchers for many decades. The research in this field has strongly profited from the development of catalytically competent well-defined transition metal complexes since they allow for profound mechanistic studies. Single-site water oxidizing catalysts (WOC) have gained strong interest, starting with the synthesis and characterization of the first active mononuclear ruthenium complex by Thummel et al.[1] Subsequent mechanistic studies by Meyer et al.[2-4] have led to a proposal of the catalytic pathway in which the key O-O bond formation step results from a water nucleophilic attack on the Ru^{V}=O unit (Figure 1). It is assumed that this mechanism holds for a variety of mononuclear Ru catalysts from $[Ru(trpy)(bpy)(H_2O)]^{2+}$ (**1^{2+}**) (where trpy is 2,2':6',2"-terpyridine and bpy is 2,2'-bipyridine) analogues[5,6] to single site Ru polyoxometalates,[7] and may also provide a description of molecular catalysts involving iridium[8] and other first-row transition metals.[9,10] Substantial efforts have been made to identify the proposed metal peroxido and hydroperoxido intermediates and possible side products via EPR, UV-vis and vibrational spectroscopy. However, a comprehensive characterization of all intermediates and an unambiguous confirmation of the mechanism has not been achieved up to now.[3,11] Additional information can be derived from kinetic analyses, extended to compounds with modifications in the ligand framework. For instance, Fujita et al.[12] and Yagi et al.[13] have examined the effect of a pendant base on catalytic water oxidation. They found a drastic decrease of the activity when the base is placed next to the aquo ligand while the stereoisomeric complex with a distant pendant base displays an improved catalytic performance compared to **1^{2+}**. We have also studied the remarkable effect exerted by a proximal fluorine atom on the Ru-aqua group of the complex.[6] The modified bipyridine ligand forms a hydrogen bond with the active site which lowers the activity. It is further worth mentioning that 2,2'-bipyridine N,N-dioxide has been observed as the main deactivation product after catalysis with **1^{2+}** and using a large excess of $[(NH_4)_2Ce(NO_3)_6]$ (Ce^{IV} hereafter) as sacrificial oxidant,[14] which points to the dissociation of the bpy ligand as an important pathway of catalyst degradation. Finally Sakai et al. found kinetic

[a] A. Keidel, J. Staffa, Dr. U. Kuhlmann, Prof. Dr. P. Hildebrandt
Institut für Chemie Department
Technische Universität Berlin
Sekr. PC14, Straße des 17. Juni 135
D-10623 Berlin 1
E-mail: Hildebrandt@chem.tu-berlin.de

[b] Dr. I. López, Dr. F. Bozoglian, Dr. C. Gimbert-Suriñach, Dr. J. Benet-Buchholz, Prof. Dr. A. Llobet
Institute of Chemical Research of Catalonia (ICIQ)
Barcelona Institute of Science and Technology (BIST)
Av. Països Catalans, 16, 43007, Tarragona, Spain
E-mail: allobet@iciq.cat

[b] Prof. A. Llobet
Departament de Química
Universitat Autònoma de Barcelona
Cerdanyola del Vallès, 08193 Barcelona, Spain

Supporting information for this article is given via a link at the end of the document

evidence that the Ce(IV) might have a role in the O-O bond formation pathway pointing out to a different reaction mechanism.[15]

Recently, our group has demonstrated that **1**$^{2+}$ and the structurally related complex [Ru(trpy)(5,5'-F_2-bpy)(H_2O)]$^{2+}$ (where 5,5'-F_2-Bpy is 5,5'-difluoro-2,2'-bipyridine, **2**$^{2+}$) are partly converted into the new oxidatively rugged and active dinuclear catalysts [(trpy)(5,5'-X_2-bpy)Ru^{IV}(μ-O)Ru^{IV}(trpy)(O)(H_2O)]$^{4+}$ (X = H, **1-dn**$^{4+}$; X = F, **2-dn**$^{4+}$) under catalytic conditions (Figure 1).[16] This finding provided novel insight into the reactivity of so-called single-site water oxidation catalysts and did not only question the original mechanistic description of these catalysts but also disclosed the true molecular nature of the species responsible for the catalytic reaction. In this respect, two catalytic cycles run concurrently, one involving mononuclear complexes and the other one dinuclear complexes (Figure 1). The mononuclear species are irreversibly converted into the dinuclear ones via [Ru^{VI}(trpy)($O)_2$(H_2O)]$^{2+}$ (**3**$^{2+}$) that acts as a gate between the two mechanistic cycles (Figure 1).

In this work, we have studied the spectroscopic and electrochemical properties of **1-dn**$^{4+}$ and **2-dn**$^{4+}$. Using time resolved resonance Raman (RR) spectroscopy, we analysed the reactions of **1**$^{2+}$ and **2**$^{2+}$ with Ce^{IV} under stoichiometric and turnover conditions to identify intermediates of the catalytic cycle. The results are discussed on the background of the previously proposed two-cycle mechanism.[16]

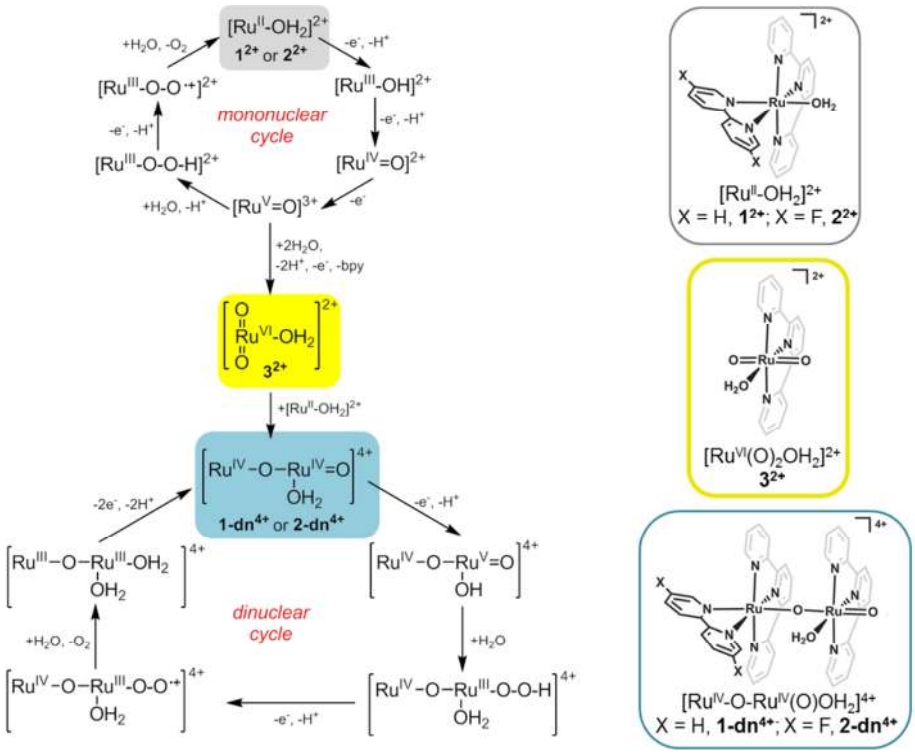

Figure 1. **Left,** Proposed reaction scheme for the water oxidation mechanisms by the monomeric Ru^{II} complexes **1**$^{2+}$, **2**$^{2+}$ and dinuclear $Ru^{IV}Ru^{IV}$ complexes **1-dn**$^{4+}$ and **2-dn**$^{4+}$, the two cycles are connected through the intermediate **3**$^{2+}$ according to previous results.[16] Polypyridyl ligands are omitted for clarity. **Right,** Structural formulas of **1**$^{2+}$, **2**$^{2+}$, **3**$^{2+}$, **1-dn**$^{4+}$ and **2-dn**$^{4+}$.

Results and Discussion

1·Synthesis and electrochemical properties of dinuclear complexes

The synthesis of the dinuclear complexes **1-dn**$^{4+}$ and **2-dn**$^{4+}$ was described previously.[16] Briefly, both compounds were prepared by reacting equimolar amounts of *trans*-[Ru^{VI}(trpy)($O)_2$(H_2O)]$^{2+}$ (**3**$^{2+}$) and the corresponding mononuclear complex, **1**$^{2+}$ and **2**$^{2+}$, in the presence of Ce^{IV} for two or three days. After filtration, the

pure dinuclear compounds are isolated in moderate yields (40 – 50 %) (Eq. 1, polypyridyl ligands not shown).

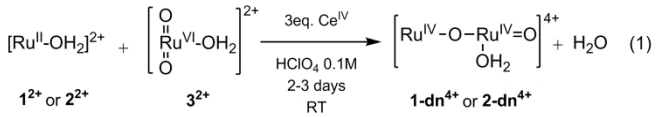

In order to characterize the different oxidation states of the dinuclear complexes, the electrochemical properties were studied within a wide range of pHs.

The CVs of **1-dn^{4+}** and **2-dn^{4+}** in 0.1 M triflic acid (pH = 1) show an electrochemically and chemically reversible wave ($E_{p,a} - E_{p,c}$ = 42 - 60 mV and $i_{p,c}/i_{p,a} \approx 1.0$) followed by a chemically irreversible wave (Figure 2). The first one is attributed to the 2-electron reduction (as determined by coulometry) of the IV,IV to the III,III oxidation state. This reduction is accompanied by a double protonation of the terminal oxo groups as indicated in Eq. 2.

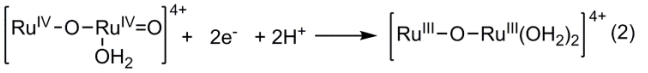

According to the relative peak height, the second wave is consistent with another two-electron reduction process from the III,III to the II,II oxidation state, which is associated with the protonation on the oxo bridge in agreement with related dinuclear III,III complexes (Eq. 3).[17-18]

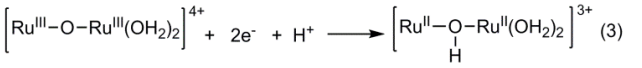

The oxidation state II,II is unstable in acidic pH and is cleaved at the oxo bridge, generating the corresponding mononuclear complexes. This is reflected by new waves emerging after a subsequent anodic scan and are thus attributed to the mononuclear compounds **3^{2+}** and **1^{2+}** (or **2^{2+}**). At pH > 4 the reduction wave becomes chemically reversible suggesting that the hydroxo-bridged complex is stable on the time scale of a CV experiment (Figure S1).

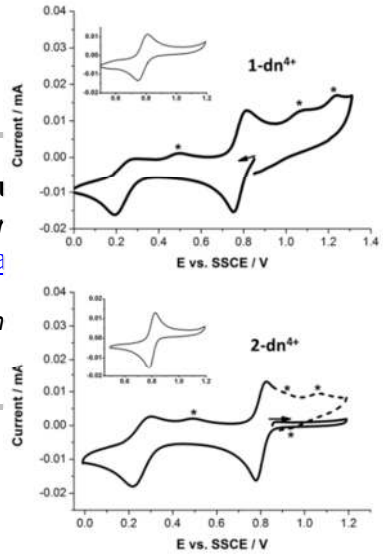

Figure 2. CVs of 0.5 mM solutions in 0.1 M triflic acid (pH 1.0) for complexes **1-dn^{4+}** (top) and **2-dn^{4+}** (bottom). The insets show CVs where the potential was switched before the irreversible reduction at E = 0.5 V. The asterisks mark electrochemical features for the mononuclear complexes. A scan rate of 100 mV s^{-1} was used.

The standard potentials for **1-dn^{4+}**, **2-dn^{4+}** and several dinuclear and mononuclear complexes are listed in Table 1. The potentials for **1-dn^{4+}**and **2-dn^{4+}** are quite similar (entry 1 *vs.* 2), despite the electron-withdrawing fluorine atoms in the bpy ring of **2-dn^{4+}** which only slightly affect the potentials (20 - 30 mV). A mixed valence state III,IV, or III.5,III.5, which might be expected in view of the strong electronic coupling through the oxo bridge,[17,20,21] is not identified in the electrochemical experiments. This suggests that E^0(III,IV/III,III) ≥ E^0(IV,IV/III,IV), i. e. the oxidation state III,IV is unstable with respect to disproportion. In contrast, the complex {[Ru(trpy)(bpy)]$_2$(μ-O)}$^{4+}$ where the terminal oxo and the aquo ligands were replaced by the bidentate bpy ligand shows only the III,IV/III,III couple in the anodic region and at higher potential (entry 5 *vs.* 1 or 2). The wave corresponding to the IV,IV/III,IV lies probably in a very high potential region where also electrode oxidation occurs. These dramatically different electrochemical properties reveal that the two aquo ligands in the oxidation state III,III of **1-dn^{4+}** or **2-dn^{4+}** play a crucial role in lowering the potentials since building-up a positive charge after oxidation can be avoided by proton-coupled electron transfer processes. Furthermore, the trans dioxo coordination in the oxidation state IV,IV stabilizes this species, contributing to a lowering of the potentials.[21,22]

The two-electron reduction wave assigned to the III,III/II,II couple in **1-dn^{4+}** and **2-dn^{4+}** indicates that E^0(II,III/II,II) ≥ E^0(III,III/II,III) such that the mixed valence state II,III is unstable with respect to disproportion. Such a behavior in water has already been observed for previously reported dinuclear oxo-bridged complexes (entries 1 or 2 *vs.* 5).[17,18] The pH-dependence of the potential for this couple shows that a proton is added upon reduction (vide infra), probably by protonating the oxo bridge group to form the corresponding hydroxo bridge in the oxidation state II,II. Because the μ-oxo group is strongly basic in that species, it is stabilized by protonation and consequently the potential for the (undetectable) II,III/II,II couple is increased. The standard potentials for this couple in **1-dn^{4+}** and **2-dn^{4+}** are similar to that of {[Ru(trpy)(bpy)]$_2$(μ-O)}$^{4+}$, indicating that the electrochemical process mainly refers to the Ru-O-Ru core. On the other hand, the well-known oxo-bridged water oxidation catalyst {[Ru(bpy)$_2$(H$_2$O)]$_2$(μ-O)}$^{4+}$, the blue dimer, differs from the previously discussed structurally related complexes (entry 3 *vs.* 1, 2 or 5). It exhibits a one-electron irreversible reduction from the oxidation state III,III to II,III where the latter is unstable towards oxo bridge cleavage.

The dinuclear complex {[Ru(trpy)(H$_2$O)]$_2$(μ-bpp)}$^{3+}$ (bpp = bis(2-pyridyl)-3,5-pyrazolate) illustrates that the substitution of the oxo bridge by a rigid aromatic ligand has drastic consequences on the electrochemical properties. The standard potentials for the IV,IV/III,III and III,III/II,II couples of {[Ru(trpy)(H$_2$O)]$_2$(μ-bpp)}$^{3+}$ are higher than those for **1-dn^{4+}**and **2-dn^{4+}** (entry 4 vs. 1 or 2). This trend can be explained by simple electrostatic arguments, since the bridging ligand μ-bpp is formally monoanionic while the μ-oxo group is dianionic. It was found that the impact of this difference is more pronounced for E^0(III,III/II,II) than for

E^0(IV,IV/III,III). Thus, the low value of the potential for the III,III/II,II couple explains why the oxo-bridged dinuclear complexes are usually isolated in high oxidation states, typically III,III.

The standard potentials for the IV,IV/III,III couple in **1-dn**$^{4+}$ and **2-dn**$^{4+}$ are slightly lower than the potentials for the IV/III or IV/II couples of the related mononuclear complexes **1**$^{2+}$ and **2**$^{2+}$ (entry 1 *vs.* 6 and entry 2 *vs.* 7). However, the onset potential for the electrocatalytic current is quite similar.

The formal potentials for the reduction of **1-dn**$^{4+}$ depend on the pH due to the acid-base properties of the different oxidation states (Eq. 2 and 3). This dependence was studied over a broad pH range and is shown in the Pourbaix diagram depicted in Figure 3. The figure contains the $E_{1/2}$-pH values obtained from CV experiments.

The straight line corresponding to the IV,IV/III,III couple displays a constant slope of 59 mV/pH unit in the pH range studied here (0 - 9). This value is consistent with a two-electron reduction with the addition of two protons. Regarding the couple III,III/II,II, a slope of approximately 30 mV/pH unit is observed in agreement with a two-electron reduction accompanied by the addition of one proton. Because both couples exhibit a constant slope in the entire pH range, spectrophotometric determinations of the pKa values for the oxidation states IV,IV and III,III were carried out (Figure 4).

Table 1. Summary of reduction potentials (V *vs.* SSCE) for various dinuclear and mononuclear complexes at pH 1.

Dinuclear complexes

		E^0				
Entry	Complex[a]	III,IV/III,III	IV,IV/III,III	III,III/II,II	E_{onset}[b]	Ref.
1	**1-dn**$^{4+}$	---	0.78[d]	0.18[d,e]	1.45	Tw.[c]
2	**2-dn**$^{4+}$	---	0.80[d]	0.21[d,e]	1.47	Tw.[c]
3	{[Ru(bpy)$_2$(H$_2$O)]$_2$(μ-O)}$^{4+}$	0.79	> 1.17[f]	< 0.06[g]	---	19
4	{[Ru(trpy)(H$_2$O)]$_2$(μ-bpp)}$^{3+}$	0.88	0.98[h]	0.62	1.30	25, 26
5	{[Ru(trpy)(bpy)]$_2$(μ-O)}$^{4+}$	1.08	---	0.21[d,e]	---	27

Mononuclear complexes

		E^0					
Entry	Complex	III/II	IV/III	IV/II	V/IV	E_{onset}[b]	Ref.
6	**1**$^{2+}$	0.82	0.98	0.90	1.62	1.45	6, 24
7	**2**$^{2+}$	---	---	0.87[d]	1.68	1.48	6
8	**3**$^{2+}$	0.47	0.87	0.67	> 1.03[i]	---	22

[a] Ligand abbreviation: bpp = bis(2-pyridyl)-3,5-pyrazolate. [b] Potential refers to the value where electrocatalysis starts. [c] Tw: this work. [d] Two electron process. [e] Chemically irreversible process; the indicated potential corresponds to $E_{p,c}$ -0.015 V. [f] The oxidation state IV,IV is unstable with respect to disproportion. Thus, E^0 is estimated considering that E^0(IV,IV/III,IV) > E^0(V,V/III,IV) where the latter is 1.22 V. [g] The oxidation state II,III undergoes oxo bridge cleavage on the time scale of the CV; however, E^0(III,III/II,II) cannot be lower than E^0(III,III/II,III). [h] The wave associated with the IV,IV/III,IV couple is electrochemically irreversible; thus, $E_{1/2}$ was estimated taking $E_{p,a}$-0.03 V. [i] The oxidation state V is unstable with respect to disproportion; thus this E^0 must be larger than E^0(VI/IV) = 1.03 V.

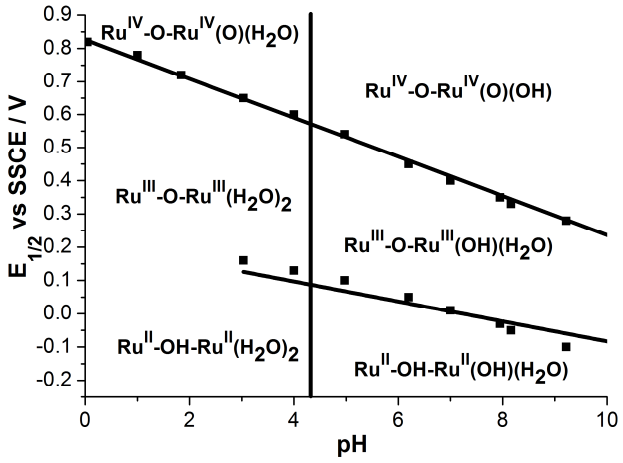

Figure 3. Pourbaix diagram for **1-dn**$^{4+}$. The potential-pH regions where the various oxidation states are the dominant forms are indicated. The vertical line represents the pK_a values obtained by spectrophotometric titrations. $E_{1/2}$ values were obtained by CV using a scan rate of 100 mV cm^{-1}.

The acid-base titration of IV,IV showed distinct isosbestic points at 363, 415, 481 and 707 nm and the pK_a(IV,IV) was calculated to be 4.4. The acid-base titration of the III,III derivative was determined using a solution of the complex obtained by coulometric reduction of the initial IV,IV form yielding a pK_a(III,III) of 4.3. In this case, the UV-Vis spectra show more subtle changes as it has been previously observed in the oxidation state III,III of the blue dimer.[18] The close similarity between both pK_a values explains why the slopes of the Pourbaix diagram for the two redox couples remain unmodified in the entire pH range. Deprotonation of IV,IV would result in a change of the slope for the redox IV,IV/III,III couple from -59 mV/pH unit (2 e$^-$/2 H$^+$ exchanged) to -29 mV/pH unit (2 e$^-$/1 H$^+$ exchanged) but deprotonation of III,III at near the same pH affords again an exchange of 2 protons in the couple. Instability of **1-dn**$^{4+}$ above pH 9.50, probably because of dimerization reactions, prevents us from obtaining reliable measurements at basic pHs.

The pK_a for the oxidation state IV,IV of **2-dn**$^{4+}$ was also determined spectrophotometrically in order to gain insight into the influence of the bpy ligand on the acid-base properties of the dinuclear complexes (Figure S2). The calculated pK_a (4.0) is lower than that found for **1-dn**$^{4+}$ as expected from the electron-withdrawing effect of the fluorine substituents in the bpy ligand. The same behavior has been reported for the mononuclear parent complexes **1**$^{2+}$ and **2**$^{2+}$.[6] However, the effect is smaller in the dinuclear complexes because the bpy ligand has a weaker influence on the electronic structure of the complex as evidenced by the standard potentials (Table 1) and the UV-vis spectra (Figure S3 and Table S1).

The pK_a value associated with the oxidation state II,II must be similar to that of the III,III state to account for the constant slope of this couple for the same reasons outlined above for IV,IV/III,III. However, we could not determine this quantity due to the previously discussed instability of this oxidation state with respect to oxo bridge cleavage. The release of the proton is ascribed to one of the aquo ligands rather than from the hydroxyl group, in line with conclusions drawn from studies of structurally related complexes.[17]

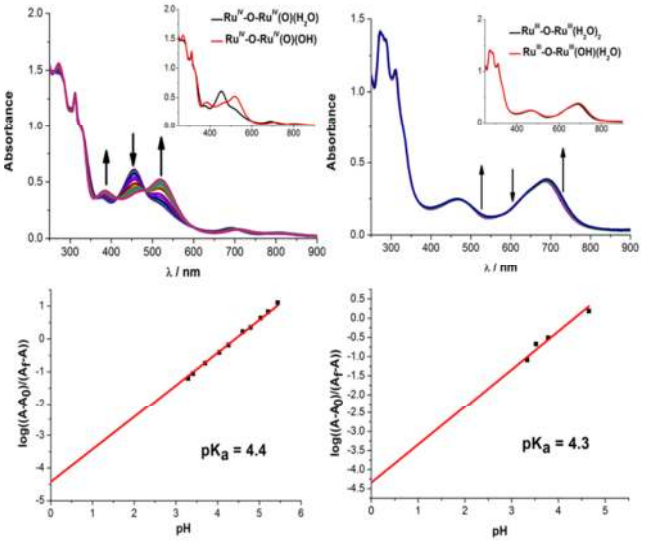

Figure 4. Top, Acid-base spectrophotometric titration of the oxidation state IV,IV (left) and III,III (right) of **1-dn**$^{4+}$ after consecutive additions of 1 - 5 µL of 6.16 M NaOH to a 25 µM solution of the complex in 0.1 M H_3PO_4 / NaH_2PO_4 buffer at pH 2.15. pH changes for the titration of IV,IV: 2.32, 2.52, 2.78, 3.29, 3.41, 3.70, 4.04, 4.26, 4.60, 4.79, 5.03, 5.21, 5.44, 5.73 and 5.95. pH changes for the titration of III,III: 2.94, 3.33, 3.52, 3.78, 4.65 and 5.22. **Bottom,** Calculation of the pK_a value of the oxidation state IV,IV from the absorbance at 519 nm (left) and of the oxidation state III,III from the absorbance at 727 nm (right).

The interpretation of the Pourbaix diagram (Figure 3) is supported by the RR spectra of the oxidation states IV,IV and III,III (Figure 5). The spectrum of IV,IV, obtained with 514 nm laser excitation, is dominated by a strong band at 803 cm^{-1}. In our previous work, this band was assigned to a mode including the stretching of the terminal Ru=O bond, consistent with the ca. 40 cm^{-1} ^{18}O/^{16}O isotopic shift.[16] A closer inspection reveals an additional weak band on the high-frequency side (833 cm^{-1}) which also falls into the region expected for Ru=O stretching. Upon 413 nm laser excitation, this latter band is preferentially

enhanced compared to the 803 cm^{-1} band. Thus, we conclude that the Ru=O and Ru-O-Ru stretching coordinates are strongly coupled, giving rise to two closely spaced modes at 803 and 833 cm^{-1} with different excitation profiles. Conversely, no $^{18}O/^{16}O$-sensitive bands were observed in the region between 350 and 400 cm^{-1}. Thus, the RR spectroscopic signature of the Ru=O and Ru-O-Ru containing modes is quite different in the IV,IV state of **1-dn^{4+}** as compared to the corresponding ruthenium "blue dimer" species which displays "pure" (symmetric) Ru-O-Ru and Ru=O stretching modes at ca. 369 and 818 cm^{-1} respectively, in its formal V,IV oxidation state.[28,29]
Upon reduction of the IV,IV form of **1-dn^{4+}** to the III,III state by addition of 2 equivalents of Mohr's salt, $(NH_4)_2Fe(SO_4)_2$, the RR intensities of the bands at 803 and 833 cm^{-1} are strongly decreased (Figure 5C) consistent with the lack of a Ru=O function as concluded from the Pourbaix diagram (Figure 3).

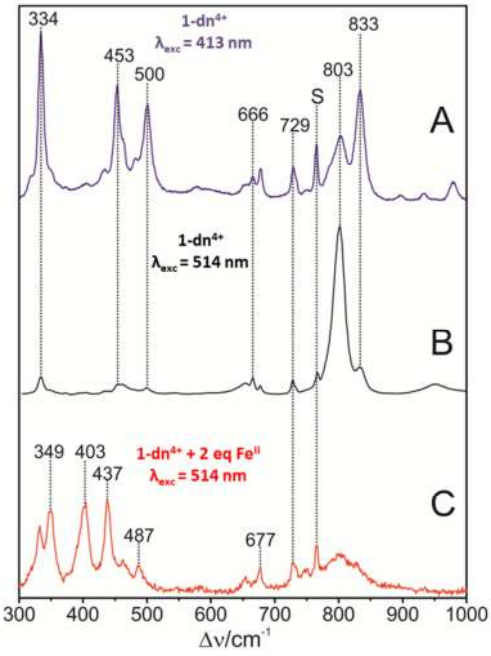

Figure 5. RR spectra of **1-dn^{4+}** in the oxidation state IV,IV obtained with (**A**) 413 nm (blue) and (**B**) 514 nm excitation (black), compared with the RR spectrum of (**C**) the III,III form of the complex, generated after the addition of 2 equivalents of $(NH_4)_2Fe(SO_4)_2$ to the **1-dn^{4+}** (red), 514 nm excitation. "S" refers to a Raman band of triflic acid. Details of the RR experiments are given in the text.

2·The Ru^{IV}=O reactive intermediate

Critical species of single-site Ru-pyridyl type of catalysts are the corresponding high oxidation states derived from the initial Ru^{II}-OH_2 state, namely Ru^{IV}=O and Ru^{V}=O (Figure 1). Here we succeeded to obtain single crystals suitable for X-Ray diffraction analysis of the Ru^{IV}=O intermediate $[Ru^{IV}(O)(trpy)(5,5'\text{-}F_2\text{-}Bpy)]^{2+}$ that is obtained from the removal of two protons and two electrons from **2**$^{2+}$. The corresponding ORTEP plot is shown in Figure 6. The structure consists of a Ru^{IV} with distorted octahedral geometry with coordinated trpy, bpy and terminal oxo ligands. The oxo ligand displays a Ru-O distance of 1.85 Å that confirms its double bond character as it falls within the range of previously reported related complexes.[27,30-36] The complex crystallizes with a solvent water molecule that is hydrogen bonded to the oxygen atom of the Ru=O group (O_{oxo}-O_{water} = 2.674 Å; O_{oxo}-H = 1.982 Å; O_{water}-H = 0.859 Å; O_{oxo}-H-O_{water} = 136.59º). A particularly interesting feature of the structure is the remarkable elongation of the Ru-N bpy bond of 2.14 Å located *trans* to the Ru=O group. The same bond for the reduced complex $[Ru^{II}(trpy)(5,5'\text{-}F_2\text{-}bpy)(H_2O)]^{2+}$ (**2**$^{2+}$) is only 2.02 Å.[6] These striking differences reflect the weakness of this Ru-N bond, favoring bpy decoordination and water substitution as we and others have suggested earlier.[14,16] An even larger effect would be expected for the one electron oxidized species Ru^{V}=O, that is proposed to undergo this bpy loss to generate **3**$^{2+}$ as shown in Figure 1.

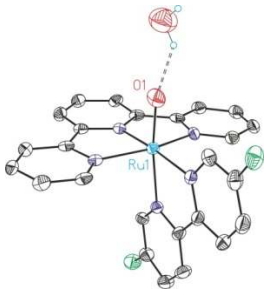

Figure 6. ORTEP plot (ellipsoid drawn at 50% probability) of the X-ray diffraction structure of dication $\{[Ru^{IV}(O)(trpy)(5,5'\text{-}F_2\text{-}bpy)]\cdot H_2O\}^{2+}$ generally indicated as $[Ru^{IV}=O]^{2+}$ in Figure 1. Color codes: Ru, cyan; O, Red; N, Blue; C, black; F, green. H atoms are not shown except for a crystallized water molecule forming a H-bond with the oxo group.

3·Time-dependent resonance Raman (RR) experiments

RR spectra of the mononuclear complexes **1**$^{2+}$ and **2**$^{2+}$ were measured with 413 nm laser excitation which is in resonance with a metal-ligand charge transfer transition[5] presumably involving the bidentate ligand (Figure 7A). As a consequence, the vibrational band patterns differ quite substantially for **1**$^{2+}$ and **2**$^{2+}$ in the entire spectral range. Here we focused on the region below 1000 cm^{-1} to monitor the modes containing coordinates of

the oxygen ligands. For the reduced parental species, these modes are not detectable as verified by the lack of any $^{18}O/^{16}O$- and $^{2}H/^{1}H$-sensitive bands.

3·1·Stoichiometric oxidation of Ru^{II} complexes

We first studied the stoichiometric oxidation of $\mathbf{1}^{2+}$, using two equivalents of Ce^{IV} (Figure 7, left). Immediately after addition of the oxidant, the band intensities of the Ru^{II} complex (i.e., at 667, 676, and 729 cm^{-1}) strongly decreased with respect to the solvent band whereas new bands at 719, 798, and 919 cm^{-1} appeared (Figure 7B). The stoichiometric oxidation of $\mathbf{2}^{2+}$ (Figure 7, right) offers a similar picture as far as the intensity loss of the Ru^{II} bands and the concomitant increase of the product bands at 657, 719, 800, 879, and 919 cm^{-1} are concerned (Figure 7B). Like the 798 cm^{-1} band of the oxidation product of $\mathbf{1}^{2+}$, the band at 800 cm^{-1} of $\mathbf{2}^{2+}$ has decayed after 24 h (Figure 7C). The temporal evolution of these bands after addition of Ce^{IV} indicates that the stoichiometric oxidation of the mononuclear complexes involves two spectroscopically detectable states, characterized by the bands with red and green colored labels in Figure 7 B,C. Essentially the same results were obtained upon addition of three instead of two oxidation equivalents, except for a faster decay of the 800 (798) cm^{-1} bands (red label) and a somewhat larger contribution of the "green" species compared to the parent states.

This band at 800 cm^{-1} is of particular interest since it can be assigned to the mononuclear Ru^{IV}=O or Ru^{V}=O species (see scheme in Figure 7, red labels), in line with the assignment for related dinuclear complexes **1-dn**$^{4+}$ and **2-dn**$^{4+}$ also containing a Ru=O group (see Figure 5, *vide supra*).[16] Indeed, isotopic labeling experiments using $H_2{}^{18}O$ show the expected 40 cm^{-1} shift of the Ru=O resonance from 800 cm^{-1} to 760 cm^{-1} (Figure S4).

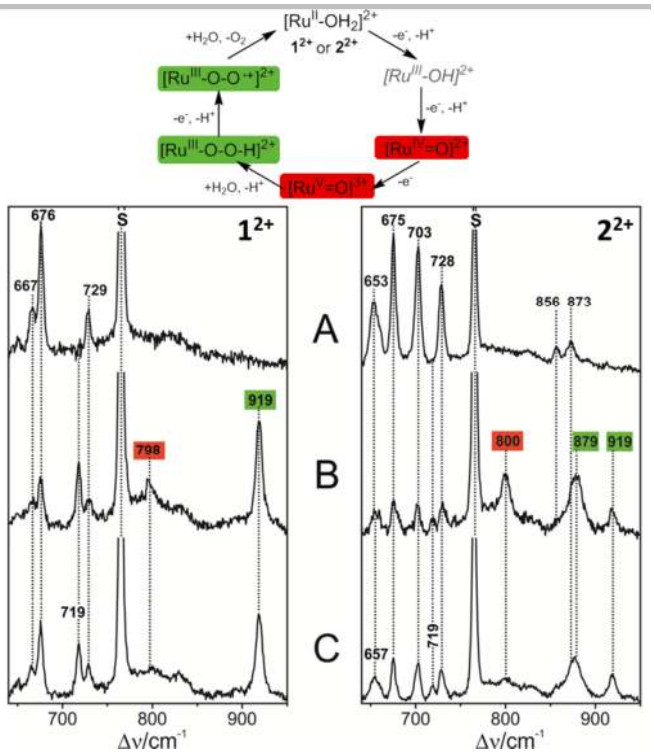

Figure 7. RR spectra of $\mathbf{1}^{2+}$ and $\mathbf{2}^{2+}$ measured upon stoichiometric oxidation with 2 equivalents of Ce^{IV}. (**A**) parental reduced Ru^{II} state; (**B**) 30 seconds after addition of Ce^{IV}; (**C**) 24 h after addition of Ce^{IV}. The spectra were obtained with 413 nm excitation at room temperature. "S" refers to a Raman band of triflic acid. The color code of the RR band labels is related to the reaction scheme indicated at the top of the figure.

The nature of the oxidized species with resonances at 879 cm^{-1} (only for $\mathbf{2}^{2+}$) and 919 cm^{-1} (for both $\mathbf{1}^{2+}$ and $\mathbf{2}^{2+}$) was assessed through the stoichiometric oxidation of $\mathbf{2}^{2+}$ in pure $H_2{}^{16}O$ or $H_2{}^{18}O$, and a 1:1 mixture of $H_2{}^{16}O$ and $H_2{}^{18}O$ (Figure 8). In this case, the $^{18}O/^{16}O$ shift was only 6 cm^{-1} and thus much smaller than that expected for a Ru=O containing modes (ca. 40 cm^{-1} band).[16] For the 1:1 mixture of $H_2{}^{16}O$ and $H_2{}^{18}O$, a broad peak is observed that evidently involves more than one band. The 919 cm^{-1} band lies within the range of the O-O fragment stretching modes for which quite different values of $\Delta\upsilon$ have been observed in the past.[11,28] Although typical isotopic shift values of ca. 50 cm^{-1} are expected for a $^{18}O/^{16}O$ substitution in the O-O fragment, distinctly smaller shifts below 20 cm^{-1} have been reported for Ru compounds that were assigned to peroxo or superoxo derivatives.[11] Such small shifts suggest a distribution of the O-O stretching coordinate and thus of the isotopic shift among several modes. Accordingly, this 919 cm^{-1} band can be ascribed to the O-O stretching of either the Ru^{III} hydroperoxo [Ru^{III}-O-O-

H]$^{2+}$ or the Ru^{III} superoxo [Ru^{III}-O-O$^{\bullet}$]$^{2+}$ intermediates (indicated as green labels in the catalytic cycle depicted in Figure 7),[16] which is in line with a previous suggestions.[3,15a] Moreover, the H/D sensitivity of this band favors the assignment to the hydroperoxo complex although the H/D shift cannot be determined precisely (Fig. S5). All other bands originating from the same peroxido complex, are attributed to modes of the polypyridyl ligands since they did not display any $^{18}O/^{16}O$ shift and are found at similar position as their counterparts in the parent (reduced) complexes.

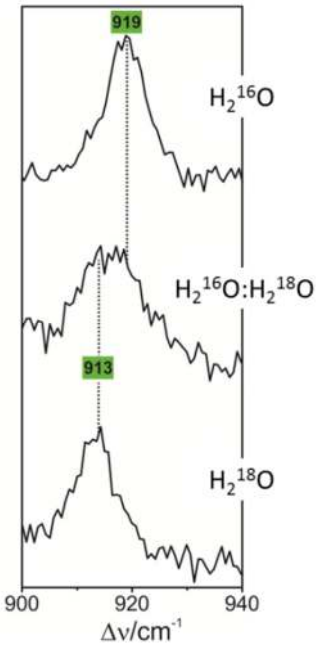

Figure 8. Section of the RR spectrum associated with the "O-O" fragment. The spectra were obtained from solutions of **2**$^{2+}$ and measured 24 hours after the addition of 2 equivalents of Ce^{IV} in $H_2{}^{16}O$ (top), in a 1:1 mixture of $H_2{}^{18}O/H_2{}^{16}O$ (middle) and in $H_2{}^{18}O$ (bottom). The green color of the band labels is related to the reaction scheme in Figure 7.

3·2·Oxidation of Ru^{II} complexes under turnover conditions

We studied the oxidation of the mononuclear complexes **1**$^{2+}$ and **2**$^{2+}$ under turnover conditions, i.e. at a large (100-fold) excess of Ce^{IV}. This process is accompanied by the clearly visible evolution of O_2. Spectra were measured consecutively each 30 minutes after addition of the oxidant. Both complexes display the same time-dependent behavior as illustratively shown for the oxidation of **1**$^{2+}$ (Figure 9). Thirty minutes after Ce^{IV} addition, the characteristic bands of **1**$^{2+}$, such as that at 676 cm^{-1}, have disappeared and new bands at 835 and 717 cm^{-1} have grown in. After one hour, an additional band emerges at 799 cm^{-1} and after ca. two hours the process has evidently reached equilibrium concentrations. Thus, under turnover conditions, two different Ru species are detectable in the RR spectra, an "early" intermediate and a final product with the color labels yellow and blue, respectively (Figure 9). No signal at 919 cm^{-1} attributed to the O-O vibration was observed in any of the spectra.

To identify these two species, the RR spectra of the reaction mixture at early (30 min) and late times (120 min) were compared with those of separately synthesized and purified Ru reference complexes (Figure 10). Complex **3**$^{2+}$**,** that is suggested to be the intermediate connecting the monomeric and the dimeric water oxidation reaction cycles, shows a simple RR spectrum with only five bands in the range between 300 and 900 cm^{-1}(Figure 10B, yellow label). Four rather weak bands that are at positions very similar to those of **1**$^{2+}$, i.e. at ca. 685, and 734 cm^{-1}, most likely originate from vibrational modes of the trpy ligand (compare Figure 10A and 10B). The most intense band is observed at 835 cm^{-1} and is readily attributed to a mode including the O=Ru=O stretching coordinate.[21] Only this mode can be identified in the "early" RR spectrum of the catalytic process, implying that soon after the addition of excess Ce^{IV} the Ru^{VI}-dioxo complex **3**$^{2+}$ is formed. With increasing time, the 835 cm^{-1} band broadens concomitant to the growing-in of the 799 cm^{-1} band. The unusually broad shape of the 835 cm^{-1} band indicates the involvement of several components with similar frequencies. The comparison with the RR spectrum of isolated **1-dn**$^{4+}$ suggests that it is this dimer and closely related species (compare Figure 10D and 10E, blue labels) that dominate the RR spectrum at "late" times. Note that the 833 cm^{-1} band of the isolated and purified dimer **1-dn**$^{4+}$ is slightly lower in frequency than the O=Ru=O stretching mode of **3**$^{2+}$ (835 cm^{-1}). Thus, it may well be that residual contributions of **3**$^{2+}$ species also contribute to the broadening of 835 cm^{-1} band.

3·3·Implications for the reaction mechanism

Time-resolved RR spectroscopy of a chemical reaction probes the actual composition of the sample solution at given delay times with respect to the addition of the oxidant. However, the RR spectra do not reflect the true relative concentrations of the reaction mixture, since at a given excitation line the relative and absolute Raman cross sections of the individual species may be quite different. For this reason and due to unfavorable kinetics not all intermediate states that are involved can be detected in the time-dependent RR experiments. For instance, the primary oxidation product of Ru^{II}-OH_2, i.e. Ru^{III}-OH (or Ru^{II}-OH_2 at pH 1), is not detected at any time, although it has to be transiently formed as proven by EPR spectroscopy.[11b]

We first consider the stoichiometric oxidation of Ru^{II} which requires hours to reach the chemical equilibrium. In the presence of 2 and 3 equivalents of Ce^{IV} the originally proposed reaction scheme (Figure 1) implies that the reaction can only run up to the Ru^{IV}=O and Ru^{V}=O complexes. While the latter is EPR active, the first is EPR silent so the best way to detect it is by using rR spectroscopy due to strong signature of the Ru=O vibrations. In fact, in both cases (2 and 3 equivalents of Ce^{IV}) we note the formation of a Ru=O species from $\mathbf{1}^{2+}$ and $\mathbf{2}^{2+}$ in the first spectra measured immediately after addition of the oxidant (Figure 7B). These reactions may be rather fast (minute time scale). However, under these conditions the Ru=O species can slowly decay to the $[Ru^{III}\text{-}O\text{-}O^{\cdot+}]^{2+}$ or, more likely, $[Ru^{III}\text{-}O\text{-}O\text{-}H]^{2+}$ complex (Figure 7C), via the proposed disproportionation reaction indicated in Eq. 4-5.

$$2[Ru^{IV}{=}O]^{2+} + H^{+} \longrightarrow [Ru^{V}{=}O]^{3+} + [Ru^{III}\text{-}OH]^{2+} \quad (4)$$

$$[Ru^{V}{=}O]^{3+} + H_2O \longrightarrow [Ru^{III}\text{-}OOH]^{2+} + H^{+} \quad (5)$$

$$2[Ru^{IV}{=}O]^{2+} + H_2O \longrightarrow [Ru^{III}\text{-}OOH]^{2+} + [Ru^{III}\text{-}OH]^{2+} \quad (4) + (5)$$

A pathway that we have previously found and discussed for related complexes.[37] However other potential pathways for the generation of $[Ru^{III}\text{-}O\text{-}O\text{-}H]^{2+}$ involving Ce^{IV} may exist as proposed by Sakai et al. [15]

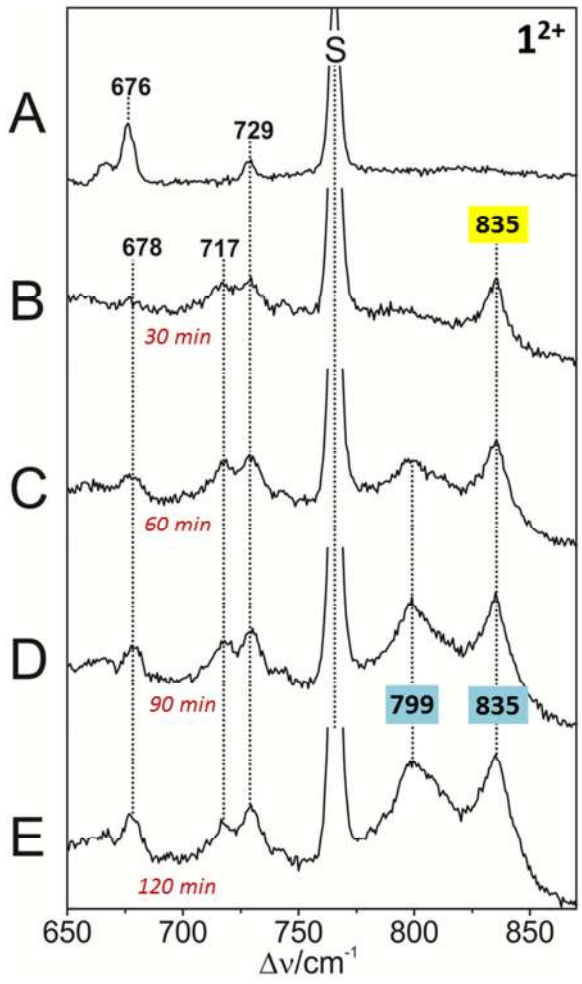

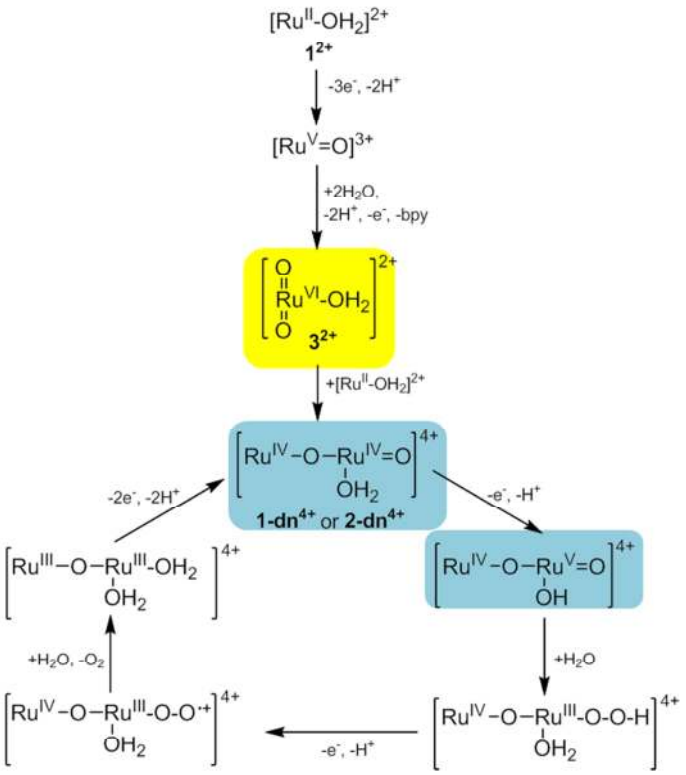

Figure 9. RR spectra of $\mathbf{1}^{2+}$ measured upon oxidation with excess (100 equivalents) of Ce^{IV}. (**A**) parental reduced Ru^{II} state; (**B**) 30 min after addition; (**C**) 60 min after addition; (**D**) 90 min addition; (**E**) 120 min after addition. The spectra were obtained with 413 nm excitation at room temperature. "S" refers to a Raman band of triflic acid. The color code of the band labels is related to the reaction scheme depicted in the right of the figure.

This finding also implies that the monomeric $\mathbf{1}^{2+}$ and $\mathbf{2}^{2+}$ complexes are catalytically competent insofar as they catalyse O-O bond formation from water. The identification of the O_2-releasing state to a Ru^{III} (superoxo) hydroperoxo complex confirms previous suggestions in the literature.[3,15a]

This disproportionation reaction seems to play only a minor role upon oxidation of Ru^{II} with large excess of Ce^{IV} as the signal attributed to $[Ru\text{-}O\text{-}O]^{n+}$ type of complexes is very weak under these conditions (Fig. S6). The spectrally prevalent species at early times is instead the *trans*-dioxo Ru^{VI} complex $\mathbf{3}^{2+}$ that according to the proposed scheme links the monomeric and dimeric reaction cycle (Figure 1 and 9). Using a 100-fold excess of Ce^{IV}, the reaction runs repetitively through the dinuclear cycle under evolution of O_2. Here the RR spectra only reveal contributions from $\mathbf{1\text{-}dn}^{4+}$ and $\mathbf{3}^{2+}$ (Figure 9 and 10). The failure to detect other intermediates of the reaction scheme may either be due to their low resonance enhancement or their short lifetime due to fast decay kinetics. Consequently, the species contributing to the RR spectra measured during turnover and after consumption of all oxidizing equivalents are nearly the same. It is important to keep in mind that the RR analysis does not provide a quantitate analysis related to the relative amount of the species in the reaction sequence and thus only give a qualitative picture.

Altogether, the results of the present study are fully consistent with the previously proposed reaction scheme (Figure 1), demonstrating that formation of dinuclear complex $\mathbf{1\text{-}dn}^{4+}$ is essential for an efficient catalytic process, especially if long lasting performance is needed for potential technological applications.

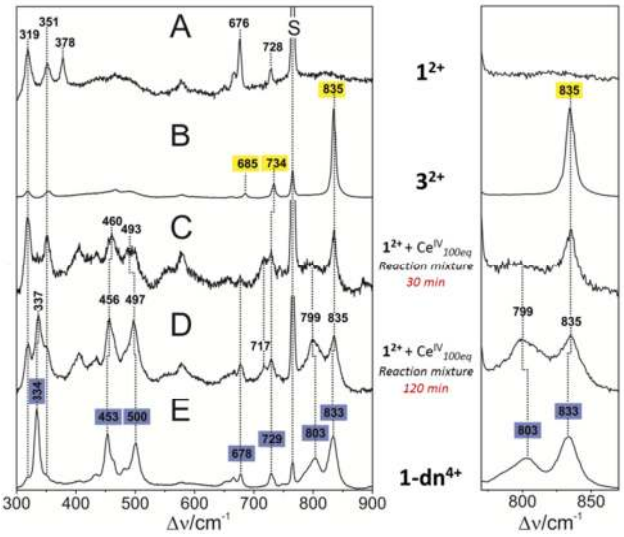

Figure 10. RR spectra of $\mathbf{1}^{2+}$ measured upon oxidation with excess (100 equivalents) of Ce^{IV}, compared with the RR spectra of reference complexes. (**A**) pure $\mathbf{1}^{2+}$; (**B**) pure $\mathbf{3}^{2+}$; (**C**) $\mathbf{1}^{2+}$, 30 min after Ce^{IV} addition; (**D**) $\mathbf{1}^{2+}$, 120 min after Ce^{IV} addition; (**E**) pure $\mathbf{1\text{-}dn}^{4+}$. The right panel shows the RR spectra between 770 and 870 cm^{-1} on an expanded view. The spectra were obtained with 413 nm excitation at ambient temperature. "S" refers to a Raman band of triflic acid. The color code of the band labels is related to the reaction scheme in Figure 9.

Conclusions

In a previous study we demonstrated that single-site WOCs structurally related to $\mathbf{1}^{2+}$ evolved to oxo-bridge dinuclear complexes which are rugged catalysts. The presented work constitutes a mandatory continuation where the electrochemical and acid-base properties of the dinuclear compounds $\mathbf{1\text{-}dn}^{4+}$ and $\mathbf{2\text{-}dn}^{4+}$ have been thoroughly examined. $\mathbf{1\text{-}dn}^{4+}$ shows two pH-dependent 2 electron waves in cyclic voltammetry. The wave attributed to the IV,IV/III,III couple is associated with the double protonation of the terminal oxo ligand of IV,IV according to the Pourbaix diagram. The second wave proceeds from the III,III/II,II couple and is associated with protonation of the oxo bridge ligand according to its pH-dependency. The pK_a values of the aquo ligands in IV,IV and III,III were determined spectrophotometrically. Both values are quite similar (pK_a(IV,IV) = 4.4 and pK_a(III,III) = 4.3), accounting for the constant slope for

the two couples in the Pourbaix diagram. Additionally, the pK_a for the IV,IV oxidation state of **2-dn^{4+}** was found to be slightly lower than that for **1-dn^{4+}** (4.0 *vs.* 4.4), which is consistent with the electron-withdrawing effect exerted by the fluorine atoms of the bpy ligand.

The conversion of **1^{2+}** to **1-dn^{4+}** was studied thoroughly by *in situ* RR spectroscopy after the addition of stoichiometric amounts or an excess, that is under catalytic conditions, of Ce^{IV}. In the first case we have observed two different species which can be assigned to $[Ru=O]^{n+}$ and $[Ru\text{-}O\text{-}O]^{n+}$ type of complexes. Under turnover conditions, the intermediate appearing immediately after the addition of the oxidant was unambiguously identified as the *trans*-dioxo complex **3^{2+}**. The second species that accumulated later during catalytic turnover is the crucial dinuclear complex **1-dn^{4+}**. These findings support our previously proposed mechanism and complete the characterization of most of the envisaged intermediates.

Finally, the X-Ray structure of the oxidation state IV from **2^{2+}** evidences the proposed *trans* effect exerted by the oxo group and that eventually leads to the release of the bpy ligand and the consecutive formation of **3^{2+}**. This critical process constitutes the origin of the formation of the highly rugged dinuclear WOCs **1-dn^{4+}** and **2-dn^{4+}**.

Experimental Section

Materials. $RuCl_3 \cdot 3H_2O$ was supplied by Alfa Aesar and was used as received. Trifluoromethanesulfonic acid (HOTf) was purchased from CYMIT. All other reagents used in the present work were obtained from Aldrich Chemical Co. and were used without further purification. Reagent-grade organic solvents were obtained from SDS and high-purity deionized water was obtained by passing distilled water through a nanopure Milli-Q water purification system.

Preparations. $[Ru^{II}(trpy)(bpy)(H_2O)](PF_6)_2$ (**1^{2+}**),[23] $[Ru^{II}(trpy)(5,5'\text{-}F_2\text{-}bpy)(H_2O)](PF_6)_2$ (**2^{2+}**),[6] *trans*-$[Ru^{VI}(trpy)(O)_2(H_2O)](PF_6)_2$ (**3^{2+}**),[21] $[(trpy)(bpy)Ru^{IV}(\mu\text{-}O)Ru^{IV}(trpy)(O)(H_2O)](ClO_4)_4$ (**1-dn^{4+}**),[16] and $[(trpy)(5,5'\text{-}F_2\text{-}bpy)Ru^{IV}(\mu\text{-}O)Ru^{IV}(trpy)(O)(H_2O)](ClO_4)_4$ (**2-dn^{4+}**)[16] were prepared as described in the literature. *Warning. Perchlorate salts are hazardous because of the possibility of explosion. They should be prepared in small amounts, stored appropriately and not warmed above 40°C.*

Samples for RR spectroscopy using 514 nm excitation were prepared by mixing a 1 mM solution of **1-dn^{4+}** in 0.1 M triflic acid (pH 1.0) with two equivalents of $(NH_4)_2Fe(SO_4)_2$ (Fe^{II} in text). 100 µL of the reaction solution were transferred to an aluminium crucible and subsequently frozen in liquid N_2. Then, the crucible was placed into a Linkam THMS 600 temperature-controlled cryostage to keep the temperature at -12 °C. For RR measurements using 413 nm excitation, the complexes were dissolved in triflic acid at pH 1.0 with a concentration of 1 mM. Spectra were measured at ambient temperature. For determining $^{18}O/^{16}O$ isotopic shifts, the experiments were carried out in $H_2{}^{16}O$, $H_2{}^{18}O$, and 1:1 mixtures of $H_2{}^{16}O$ and $H_2{}^{18}O$. Oxidation of the Ru(II) complexes was achieved by addition of $[(NH_4)_2Ce(NO_3)_6]$ (Ce^{IV} in text).

Methods. UV/Vis spectroscopy was carried out with a Cary 50 (Varian) UV/Vis spectrophotometer. Cyclic voltammetry (CV) and differential pulse voltammetry (DPV) experiments were performed using a IJ-Cambria CHI-660 or a Bio-Logic SP-150 potentiostat controlling a three-electrode cell. Typical CV experiments were carried out at a scan rate of 100 mV s^{-1}. For DPV experiments, we used a pulse height and width of 50 mV and 50 ms, respectively. The step height and step time was set to 4 mV and 200 ms, respectively. A glassy carbon electrode (3 mm diameter) was used as working electrode, platinum wire as auxiliary electrode, and a SSCE or Hg/Hg_2SO_4 (sat. K_2SO_4) as reference electrode. Working electrodes were polished with 0.05 micron alumina paste and rinsed with distilled water and acetone followed by blow-drying before each measurement. For activation of glassy carbon electrodes, a procedure described by Meyer *et al.* was used.[38] All CVs presented in this work were recorded in the absence of light and inside a Faraday cage. The electrochemical experiments were carried out in 1 M HOTf (pH 0.0) or 0.1 M HOTf (pH 1.0). For higher pH values, different buffers were used, NaH_2PO_4/H_3PO_4 (pH range 2.0 – 4.0), Na_2HPO_4/NaH_2PO_4 (pH range = 4.0 – 8.0), sodium tetraborate (pH range 8.0 – 9.5). In each case, the ionic strength was set to 0.1 M. $E_{1/2}$ values reported in this work were estimated from the oxidative and reductive peak potentials in CV experiments, i.e. $(E_{p,a} + E_{p,c})/2$, or as the potential at maximum current $E(I_{max})$ in DPV measurements.

RR spectra at 514 nm excitation were measured using a Renishaw inVia Reflex RAMAN confocal microscope (Gloucestershire, UK), equipped with an Ar ion laser. The spectrometer was equipped with a Peltier-cooled CCD detector (-70°C) coupled to a Leica DM-2500 microscope. Calibration was carried out with respect to the Raman spectrum of an Si standard. Spectra were recorded with an accumulation of 5 x 20 s. A 10x working distance microscope objective was used to focus the laser beam (25 mW) onto the sample.

RR spectra with 413 nm excitation (Kr ion laser) were measured using a confocal Raman spectrometer (LabRAM HR800, Horiba), equipped with a liquid-nitrogen cooled CCD detector. The laser beam (10 mW) was focused onto the sample contained in a rotating quartz cell. The total accumulation time of the spectra was ca. 10 minutes at room temperature. The spectral resolution was ca. 2 cm^{-1}. Details of the experimental set-up were described elsewhere.[39]

Single-Crystal X-Ray Structure Determination. Single crystals of $[Ru^{IV}(O)(trpy)(5,5'\text{-}F_2\text{-}bpy)](PF_6)_2$ were grown for 4 days after the dropwise addition of an aqueous saturated NH_4PF_6 solution to a reaction mixture of 3 equivalents of Ce^{IV} and **2^{2+}** in 0.1 M HOTf that was previously left reacting for one day. All crystals were prepared under inert conditions immersed in perfluoropolyether as the protecting oil for manipulation.

Data collection. Crystal structure determination was carried out using a Apex DUO Kappa 4-axis goniometer equipped with an APPEX 2 4K CCD area detector, a Microfocus Source E025 IuS using MoK_α radiation, Quazar MX multilayer Optics as monochromator, and an Oxford Cryosystems low temperature device Cryostream 700 plus (T = -173 °C). Full-sphere data collection was used with ω and φ scans. Data collection and reduction were carried out with the programs APEX-2 and Bruker Saint19 V/.60A, respectively.[40,41]

Structure Solution and Refinement. Crystal structure solution was achieved using direct methods as implemented in SHELXTL[42] and visualized using the program XP. Missing atoms were subsequently located from difference Fourier synthesis and added to the atom list. Least-square refinement on F2 using all measured intensities was carried out using the program SHELXTL. All non-hydrogen atoms were refined including anisotropic displacement parameters.

Acknowledgements

The work was supported by the Cluster of Excellence UniCat and the IRTG 1524, funded by the DFG. A.L. thanks MINECO (CTQ-2013-49075-R, SEV-2013-0319, CTQ2014-52974-REDC), Feder Funds and AGAUR (2014 SGR 915), for financial support. The Fotofuel Network of Excellence 2014 and the EU COST actions CM1202 and CM1205 are also gratefully acknowledged. IL thanks FPU for a PhD grant.

Keywords: peroxido • resonance Raman • ruthenium • superoxido • water oxidation

[1] R. Zong and R. P. Thummel, *J. Am. Chem. Soc.* **2005**, *127*, 12802-12803.
[2] J. J. Concepcion, J. W. Jurss, J. L. Templeton and T. J. Meyer, *J. Am. Chem. Soc.* **2008**, *130*, 16462-16463.
[3] J. J. Concepcion, M.-K. Tsai, J. T. Muckerman and T. J. Meyer, *J. Am. Chem. Soc.* **2010**, *132*, 1545-1557.
[4] J. J. Concepcion, J. W. Jurss, M. R. Norris, Z. Chen, J. L. Templeton and T. J. Meyer, *Inorg. Chem.* **2010**, 49, 1277-1279.
[5] D. J. Wasylenko, C. Ganesamoorthy, M. A. Henderson, B. D. Koivisto, H. D. Osthoff and C. P. Berlinguette, *J. Am. Chem. Soc.* **2010**, *132*, 16094-16106.
[6] S. Maji, I. López, F. Bozoglian, J. Benet-Buchholz and A. Llobet, *Inorg. Chem.* **2013**, *52*, 3591-3593.
[7] M. Murakami, D. Hong, T. Suenobu, S. Yamaguchi, T. Ogura and S. Fukuzumi, *J. Am. Chem. Soc.* **2011**, *133*, 11605-11613.
[8] J. D. Blakemore, N. D. Schley, D. Balcells, J. F. Hull, G. W. Olack, C. D. Incarvito, O. Eisenstein, G. W. Brudvig and R. H. Crabtree, *J. Am. Chem. Soc.* **2010**, *132*, 16017-16029.
[9] D. J. Wasylenko, R. D. Palmer, E. Schott and C. P. Berlinguette, *Chem. Commun.* **2012**, *48*, 2107-2109.
[10] M.-T. Zhang, Z. Chen, P. Kang and T. J. Meyer, *J. Am. Chem. Soc.* **2013**, *135*, 2048-2051.
[11] (a) D. E. Polyansky, J. T. Muckerman, J. Rochford, R. Zong, R. P. Thummel and E. Fujita, *J. Am. Chem. Soc.* **2011**, *133*, 14649-14665. (b) Y. Pushkar, D. Moonshiram, V. Purohit, L. Yan, I. Alperovich, *J. Am. Chem. Soc.* **2014**, *136*, 11938-11945. (c) J. Honta, S. Tajima, T. Sato, K. Saito, T. Yui, M. Yagi, *J. Photochem. Photob. A: Chem.* **2015**, *313*, 126-130.
[12] J. L. Boyer, D. E. Polyansky, D. J. Szalda, R. Zong, R. P. Thummel and E. Fujita, *Angew. Chem. Int. Ed.* **2011**, *50*, 12600-12604.
[13] H. Yamazaki, T. Hakamata, M. Komi and M. Yagi, *J. Am. Chem. Soc.* **2011**, *133*, 8846-8849.
[14] D. J. Wasylenko, C. Ganesamoorthy, B. D. Koivisto, M. A. Henderson and C. P. Berlinguette, *Inorg. Chem.* **2010**, *49*, 2202-2209.
[15] a) A. Kimoto, K. Yamauchi, M. Yoshida, S. Masaoka, K. Sakai, *Chem. Commun.* **2012**, *48*, 239-241; b) S. Masaoka, K. Sakai, *Chem. Lett*. **2009**, *38*, 182-183.
[16] I. López, M. Z. Ertem, S. Maji, J. Benet-Buchholz, A. Keidel, U. Kuhlmann, P. Hildebrandt, C. J. Cramer, V. S. Batista and A. Llobet, *Angew. Chem. Int. Ed.* **2014**, *53*, 205-209.
[17] A. Llobet, P. Doppelt and T. J. Meyer, *Inorg. Chem.* **1988**, *27*, 514-520.
[18] A. Llobet, M. E. Curry, H. T. Evans and T. J. Meyer, *Inorg. Chem.* ***1989***, *28*, 3131-3137.
[19] J. A. Gilbert, D. S. Eggleston, W. R. Murphy, D. A. Geselowitz, S. W. Gersten, D. J. Hodgson and T. J. Meyer, *J. Am. Chem. Soc.* **1985**, *107*, 3855-3864.
[20] R. Schneider, T. Weyhermueller, K. Wieghardt and B. Nuber, *Inorg. Chem.* **1993**, *32*, 4925-4934.
[21] J. W. Jurss, J. J. Concepcion, J. M. Butler, K. M. Omberg, L. M. Baraldo, D. G. Thompson, E. L. Lebeau, B. Hornstein, J. R. Schoonover, H. Jude, J. D. Thompson, D. M. Dattelbaum, R. C. Rocha, J. L. Templeton and T. J. Meyer, *Inorg. Chem.* **2012**, *51*, 1345-1358.
[22] S. A. Adeyemi, A. Dovletoglou, A. R. Guadalupe and T. J. Meyer, *Inorg. Chem.* **1992**, *31*, 1375-1383.
[23] J. M. Mayer, *Comments Inorg. Chem.* **1988**, *8*, 125-135.
[24] K. J. Takeuchi, M. S. Thompson, D. W. Pipes and T. J. Meyer, *Inorg. Chem.* **1984**, *23*, 1845-1851.
[25] F. Bozoglian, S. Romain, M. Z. Ertem, T. K. Todorova, C. Sens, J. Mola, M. RodrìÌ guez, I. Romero, J. Benet-Buchholz, X. Fontrodona, C. J. Cramer, L. Gagliardi and A. Llobet, *J. Am. Chem. Soc.* **2009**, *131*, 15176-15187.
[26] S. Roeser, PhD Thesis, Universitat Rovira i Virgili, **2011**.
[27] I. López, S. Maji, J. Benet-Buchholz and A. Llobet, *Inorg. Chem.* **2015**, *54*, 658-666.
[28] D. Moonshiram, J. W. Jurss, J. J. Concepcion, T. Zakharova, I. Alperovich, T. J. Meyer and Y. Pushkar, *J. Am. Chem. Soc.* **2012**, *134*, 4625-4636.
[29] a) J. K. Hurst, J. Zhou, Y. Lei, *Inorg. Chem.* **1992**, *31*, 1010-1017; b) H. Yamada, J. K. Hurst, *J. Am. Chem. Soc.* **2000**, 122, 5303-5311.
[30] T. W. Welch, S. A. Ciftan, P. S. White and H. H. Thorp, *Inorg. Chem.* **1997**, *36*, 4812-4821.
[31] C. M. Che, T. F. Lai and K. Y. Wong, *Inorg. Chem.* **1987**, *26*, 2289-2299.
[32] W.-C. Cheng, W.-Y. Yu, K.-K. Cheung and C.-M. Che, *J. Chem. Soc., Dalton Trans.* **1994**, 57-62.
[33] C. M. Che, W. T. Tang, W. T. Wong and T. F. Lai, *J. Am. Chem. Soc.* **1989**, *111*, 9048-9056.
[34] T. Kojima, K. Nakayama, K. Ikemura, T. Ogura and S. Fukuzumi, *J. Am. Chem. Soc.* **2011**, 133, 11692-11700.
[35] W.-C. Cheng, W.-Y. Yu, J. Zhu, K.-K. Cheung, S.-M. Peng, C.-K. Poon and C.-M. Che, *Inorg. Chim. Acta* **1996**, *242*, 105-113.
[36] E. L. Lebeau, S. A. Adeyemi and T. J. Meyer, *Inorg. Chem.* **1998**, *37*, 6476-6484.
[37] R. Roeser, P. Farras, F. Bozoglian, M. Martínez-Belmonte, J. Benet-Buchholz, A. Llobet, *ChemSusChem* **2011**, *4*, 197-207.

[38] G. E. Cabaniss, A. A. Diamantis, W. R. Murphy, R. W. Linton and T. J. Meyer, *J. Am. Chem. Soc.* **1985**, *107*, 1845-1853.

[39] H. K. Ly, T. Utesch, I. Díaz-Moreno, J. M. García-Heredia, M. Á. De La Rosa and P. Hildebrandt, *J. Phys. Chem. B* **2012**, *116*, 5694-5702.

[40] Data collection with APEX II, v2009.1-0.2, Bruker AXS Inc., Madison, Wisconsin, USA, **2009**.

[41] Data reduction with Buker SAINT V7.60A, Bruker AXS Inc., Madison, Wisconsin, USA, **2007**.

[42] G. Sheldrick, *Acta Crystallographica Section A* **2008**, *64*, 112-122.

The conversion of single-site water oxidation catalysts of type **1**$^{2+}$ into the more rugged dinuclear derivatives of type **1-dn**$^{4+}$ has been studied with time resolved resonance Raman spectroscopy. Key intermediates of the mononuclear and dinuclear water oxidation catalytic cycles have been identified. The electrochemistry of **1-dn**$^{4+}$ has been examined in detail showing a strong pH dependent redox events. The bridging and terminal oxo ligands play a crucial role in the redox properties of the dinuclear catalysts.

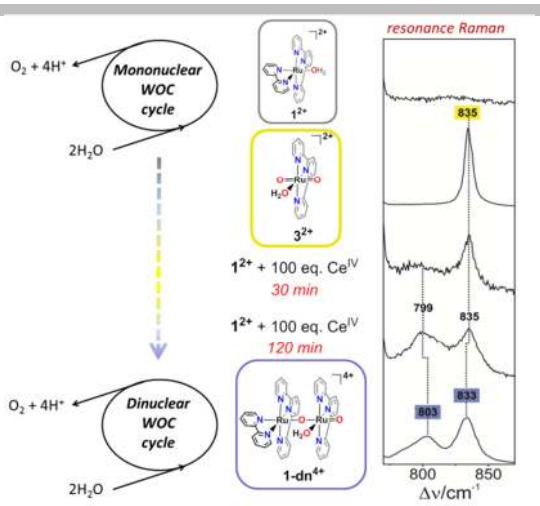

Anke Keidel, Isidoro López,Jana Staffa, Uwe Kuhlmann, Fernando Bozoglian, Carolina Gimbert-Suriñach, Jordi Benet-Bucholz, Peter Hildebrandt, and Antoni Llobet**

Page No. – Page No.

Electrochemical and Resonance Raman Spectroscopic Studies of Water-Oxidizing Ruthenium-Terpyridyl-Bipyridyl Complexes